ELSEVIER

Earth and Planetary Science Letters 205 (2002) 37–51

EPSL

www.elsevier.com/locate/epsl

Is the transition zone an empty water reservoir? Inferences from numerical model of mantle dynamics

Guillaume Richard [a,*], Marc Monnereau [a], Jannick Ingrin [b]

[a] *Observatoire Midi-Pyrénées, UMR 5562, 14 Av. E. Belin, 31400 Toulouse, France*
[b] *Laboratoire Mécanismes de Transfert en Géologie, UMR 5563, 39 Al. J. Guesde, 31000 Toulouse, France*

Received 5 July 2002; received in revised form 27 September 2002; accepted 9 October 2002

Abstract

Water is probably present everywhere in the Earth's mantle today, with abundances ranging between scales of percent (%) to the parts per million (ppm). Mantle total water content is estimated to be between 10% to several times that of the present-day hydrosphere. Numerous studies have been devoted to the determination of water solubility in mantle material [D.R. Bell, G.R. Rossmann, Science 255 (1992) 1391–1397; J. Ingrin, H. Skogby, Eur. J. Mineral. 12 (2000) 543–570]. They all show strong solubility variations from one mineral phase to another. Principally, water partitioning has made the transition zone a probable trap for water from the Earth's mantle [N. Bolfan-Casanova et al., Earth Planet. Sci. Lett. 182 (2000) 209–221; D.L. Kohlstedt et al., Contrib. Mineral. Petrol. 123 (1996) 345–357]. Nevertheless, water distribution within the mantle is still debated. We have studied the role of mantle dynamics in water distribution by modeling water transport and mantle convection in a two-dimensional (2-D) cartesian geometry. The model takes into account water partitioning between the mantle's transition zone and the upper mantle of 10:1 and between the lower mantle and the transition zone of 1:100 (i.e. respectively between olivine and spinel and spinel and post-spinel). We have modeled the mantle temperature field using depth-dependent viscosity and plate-like surface conditions. Water injection at the trench has also been simulated. Our numerical experiments suggest that diffusivity of water has to be very high, at least two orders of magnitude higher than the one experimentally determined [D.R. Bell, G.R. Rossmann, Science 255 (1992) 1391–1397; J. Ingrin, H. Skogby, Eur. J. Mineral. 12 (2000) 543–570] to significantly influence water distribution in Earth's mantle. In fact, the diffusion process is not efficient enough to balance the mixing due to mantle dynamics and to force water into the transition zone. We show that the distribution of water should be quite homogeneous throughout the mantle if advection and diffusion are the only processes involved in water transport in the mantle. This homogeneity implies that water below the transition zone could be in excess according to the lower mantle rocks solubility. This addresses the question of stability of free water in the lower mantle and its mobility by percolation process, which could be a very efficient transport process, previously unconsidered in this field of research.

Keywords: mantle convection; transition zone; water; numerical simulation

* Corresponding author. Tel.: +33-561-332-844; Fax: +33-561-332-900.
E-mail address: guillaume.richard@cnes.fr (G. Richard).

0012-821X/02/$ – see front matter © 2002 Elsevier Science B.V. All rights reserved.
PII: S0012-821X(02)01012-9

1. Introduction

Water is probably present everywhere in the Earth's mantle today, albeit sometimes at the parts per million (ppm) scale [5]. The total water content of the inner Earth could be less than 10% or as high as 100 times the water contained in the hydrosphere. In this case, water will be essentially present in the core [6] and the content of the mantle is estimated to be close to that of the hydrosphere. Nevertheless, water distribution within the mantle is not well known.

The effects due to the presence of water in the mantle are numerous. (i) The melting processes are directly affected through a decrease of rocks solidus [7,8], a change in the resulting chemical differentiation [9] and a decrease of magma viscosity and density [10]. (ii) Water content can also alter the seismic wave velocities and anisotropy [11], by influencing the seismic discontinuity for example [12]. (iii) Mantle dynamics should be affected by the variation of viscosity linked to the water content [13]. (iv) Electrical conductivity is also water-dependent [14]. All these effects, if observable, could be used to constrain the water distribution in the mantle. Unfortunately, at present only the seismic information seems exploitable in terms of water distribution [15].

The problem of water in the Earth's mantle may be addressed in two different ways. The first concerns the global amount in the mantle and its evolution with time. Lecuyer and Allemand [16] using sedimentary records, and Schubert and Reymer [17] modeling continental growth suggest that the ocean volume has not changed by more than 20% during the last billion years, so we may infer that the global water content of the mantle did not vary more than this amount. The second one is related to the spatial distribution of water in the mantle. For instance, Bonatti [18] infers that some hotspots may be more related to wet plumes than to hot plumes. In addition, the transition zone is suspected to behave as a water reservoir due to the high water solubility in minerals that compose it. To address these issues, we have to consider three important points.

1. Plate tectonics. It allows the internal water cycle to be connected to its external cycle by way of the recycling of hydrated oceanic crust in the mantle: the input flux of the system. Volcanism, especially at ridge, creates the output flux, due to the high water partitioning coefficient between melt and rocks [19].
2. The mobility of water. According to the minerals and to the pressure and the temperature conditions, water can be present in different forms: as free water, as H_2O form in hydrous minerals, or as point defects in nominally anhydrous minerals (NAMs). Below 100 km depth, hydrous minerals are no longer stable and NAMs are considered to be the main site for water storage [1,20]. Infrared (IR) spectroscopy shows that hydrogen occurs as proton H^+ and is closely associated with an oxygen ion O^{2-} to make an OH dipole. Mobility of water in NAMs is temperature-dependent but weakly phase-dependent [2]. Conversely, solubility is dependent on the mineral phase: water partitioning between NAMs varies over a large range [3]. Solubility of water in the mantle depends on the mineralogy of the mantle. This mineralogy is widely accepted [21], as having three main zones: the upper mantle (UM) consisting of garnet, olivine, Al-spinel and pyroxene, the transition zone (TZ) composed of β-phase, γ-phase, majorite and the lower mantle (LM) with perovskite and magnesiowustite. The maximum amount of water that can be dissolved is different in these three zones. The partition coefficient of water between the upper mantle and the transition zone, $D_{UM/TZ}$, is estimated to be 1:10 [4]. On the other hand, Bolfan-Casanova et al. [3] recently proposed a partition coefficient between lower mantle and transition zone, $D_{LM/TZ}$, higher than 1:100. As a consequence, it is expected that the transition zone is able to store a high amount of water in comparison with the other parts of the mantle [2,3,22,23].
3. Mantle dynamics. Convection in the Earth's mantle results in its vigorous convection and many numerical models have investigated the repartition of trace elements in the mantle by using a technique of passive tracers. However, hydrogen is well known for its strong intracrystalline diffusivity in mantle minerals (K_H),

several orders of magnitude higher than those of other chemical elements, so that transport by diffusion must be considered in the modeling of the water cycle in the mantle. Nevertheless, K_H remains small. It is estimated to be around 10^{-8} m^2 s^{-1} under the pressure and temperature conditions of the upper mantle [2], which is two orders of magnitude lower than the thermal diffusivity. The characteristic distance for the diffusion transport varies as the square root of the time scale we consider. In the case of the water, it is around 6 mm over 1 h and 60 cm over 1 year. At first glance, this appears much more than the rate of the convection, but at the time scale of the mantle dynamics, the water can diffuse only through 600 m during one million years and through less than 20 km during one billion years. As a consequence, we may expect that the transport by advection would play a major role in the distribution and the mixing of the water in the mantle, and that the diffusion acts mainly in the vicinity of the transition zone, where the high water solubility of the rocks may enhance its role. The aim of the present work is to highlight the balance between both processes.

2. The water equation

The first step is to give a conservation equation for the water content. As we will remain in the Boussinesq approximation, i.e. we will neglect the compressibility of rocks, we can use the water concentration $[H]$, instead of the water content $\rho[H]$, ρ being the rock density. The terms describing the time variation and the transport by advection are classical, but the diffusion term requires special care. The diffusion flux is controlled by the spatial variation of the chemical potential μ, so that a first general form of this equation would be:

$$\frac{\partial}{\partial t}[H] + \mathbf{u}\cdot\nabla[H] = \nabla\cdot\left(k_H \nabla\frac{\mu}{RT}\right) + S \qquad (1)$$

where $\mathbf{u} = (ux, uz)$ denotes the velocity vector of the rocks containing the water, T the temperature and R the gas constant. S is a generic term that allows us to include source or sink of water, as for example water injected at a subduction zone, or water released when melting occurs. k_H is a material property that relates the diffusion flux to the gradient of the chemical potential. As the chemical potential depends on the water concentration:

$$\mu = \mu^* + RT\cdot\ln[H] \qquad (2)$$

with μ^* the pure material chemical potential, the diffusion term can be rewritten as:

$$\nabla\cdot\left(k_H \nabla\frac{\mu}{RT}\right) = \nabla\cdot\left(\frac{k_H}{[H]}\nabla[H] + k_H \nabla\frac{\mu^*}{RT}\right). \qquad (3)$$

It contains two parts: the first one is classical, describing the effects related to the spatial variation in water concentration, whereas the second one reflects the effects due to variations in chemical composition. In the first term, $k_H/[H]$ stands for the water diffusivity which we will note as K_H, use hereafter instead of k_H, mainly because only the diffusivity is measured in laboratory experiments and appears independent of the water content. Replacing the diffusion term of Eq. 1 by the relation in Eq. 3 leads to our equation for water conservation law:

$$\frac{\partial}{\partial t}[H] + \mathbf{u}\cdot\nabla[H] = \kappa_H\Delta[H] + \kappa_H\nabla\cdot\left([H]\nabla\frac{\mu^*}{RT}\right) + S \qquad (4)$$

when the diffusivity is assumed to be constant.

2.1. Water diffusivity and boundary conditions

In fact, intra-grain water diffusivity in the upper mantle is temperature-dependent and follows the empirical law $\kappa_H = 4\times10^{-4}e^{-149000/(RT)}$ [2]. Accordingly, it varies from 4×10^{-9} m^2 s^{-1} to 1.6×10^{-8} m^2 s^{-1} when the temperature ranges from 1300°C to 1500°C, which would be expected in the upper mantle below the lithosphere. For a temperature of 500°C, K_H lies around 10^{-14} m^2 s^{-1}, so that the water flux away from the mantle through lithosphere can be neglected. As a consequence, the diffusivity may initially be assumed to be constant, the very low values of the diffusivity in the lithosphere being modeled through the

boundary condition, stating a zero flux at the top surface. Unlike for the upper mantle, the intragrain water diffusivity is very poorly constrained for the lower mantle minerals, but since it only slightly depends on the mineral composition in the upper mantle, we will assume that it will be constant throughout the whole mantle. Lastly, the water conservation equation requires a lower boundary condition. Due to the large uncertainties of the water solubility in iron, we assume a zero flux at the core–mantle boundary. In our model, water cannot escape from or enter the mantle, except via the source term S.

2.2. Water solubility

The second term of the right-hand side of Eq. 4 describes the diffusion effects due to the spatial variation of the chemical potential of pure mineral, μ^*. At the interface between two layers (the upper mantle, the transition zone or the lower mantle), the transition of mineral phase brings a variation in the chemical potential of pure minerals μ^*, inducing a partitioning of water content between both phases [24]. At equilibrium, the chemical potential must be identical in both layers [25], which leads us to write that the water concentration ratio between both layers, $[H]_1/[H]_2$, is equal to the partition coefficient $D_{1/2}$:

$$[H]_1 = [H]_2 D_{1/2}, \text{ with } D_{1/2} = \mathrm{e}^{\frac{\mu_2^* - \mu_1^*}{RT}} \tag{5}$$

This is introduced in the model through the description of the pure material chemical potential:

$$\mu^*(z) = RT\left(\frac{\ln(D_{\mathrm{UM/TZ}})}{2}\left(1-\tanh\left(\frac{z-z_{\mathrm{UM/TZ}}}{\sigma}\right)\right)\right.$$
$$\left.+\frac{\ln(D_{\mathrm{TZ/LM}})}{2}\left(1-\tanh\left(\frac{z-z_{\mathrm{TZ/LM}}}{\sigma}\right)\right)\right) \tag{6}$$

where z denotes the depth, $z_{I/J}$ the position of the phase changes and σ the half thickness of the phase change. We see on Fig. 1, where μ^* is plotted as a function of depth, that the partition coefficient between the upper mantle and the transition zone, i.e. between olivine and spinel, is fixed to 1:10 ($D_{\mathrm{UM/TZ}} = 10$) according to high-pressure experiments [4]. Between the transition zone and the lower mantle, i.e. between spinel and post-spinel, the partition coefficient is fixed to 100:1 ($D_{\mathrm{TZ/LM}} = 0.01$) according to Bolfan-Casanova et al. [3]. It is worth noting that the solubility does not affect the water diffusivity, but only the water concentration.

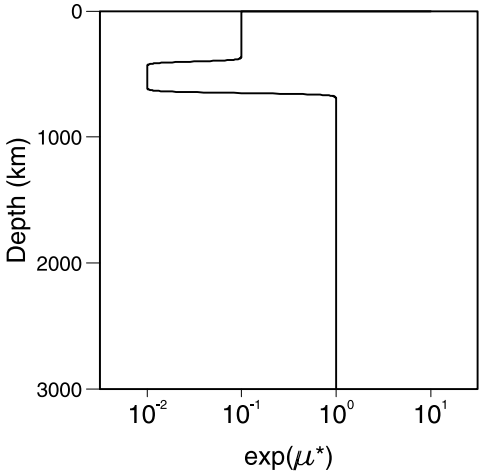

Fig. 1. Plot of the exponential value of the chemical potential of pure material as a function of depth. It can be related to water concentration following Eq. 2. In the case of pure diffusion, water concentration fits a specific profile at equilibrium induced by variation of solubility with mineral phases. We chose as the partition coefficient: 1:10 for the upper mantle/transition zone interface [4] and 1:100 for the lower mantle/transition zone interface [3].

2.3. Simple 1-D analysis

Since the dependence of the water solubility on the mineral phases is central in this problem, it is important to revisit some basics, drawn from Eq. 4, which allow us to better understand it. If we neglect the horizontal variations and assume the system will reach a steady state, Eq. 4 has an analytical solution when the pure material chemical potential behave has a step function:

$$[H]/[H]_\infty = \begin{cases} 1 + \dfrac{1-D}{D}\exp\left(\dfrac{u_z}{\kappa_{\mathrm{H}}}z\right) & \text{for } z<0 \\ 1 & \text{for } z>0 \end{cases} \tag{7}$$

where $[H]_\infty$ is the value for $[H]$ set when $z \to +\infty$.

This solution is given for a single chemical potential step located at $z=0$, in an infinite medium, where the vertical velocity, u_z, is positive (downward on Fig. 2). u_z is constant throughout the medium as to satisfy the mass conservation, $\nabla\cdot\mathbf{u}=0$. Without advection transport, $u_z=0$, the water concentration is described by a Heaviside function: $[H]=[H]_\infty/D$ above the chemical step and $[H]=[H]_\infty$ below. This directly reflects the equilibrium of the chemical potential between both layers stated in Eq. 5. In presence of advection, $u_z\neq 0$, the conservation of water prescribes that the water concentration should tend to the same value, $[H]_\infty$, when $z\rightarrow+\infty$. This analytical solution is shown by a thick curve on Fig. 2, where $D=0.01$. The step in pure material chemical potential imposes that the contrast in water concentration across the interface should be maintained equal to D, so that there is an accumulation of water above the interface. By looking at Eq. 4, we can see that the second term of the right-hand side acts as a sink term just beneath the interface, transferring the water to a source term just above. Note that, if the velocity was negative, the solution would be characterized by a defect in water content below the interface, and a constant value above. This notable effect of the step in pure material chemical potential behaves as a barrier for the water. K_H/u_z has the dimension of a length and represents the characteristic thickness of the water accumulation. It is only 30 m for $u_z=1$ cm/yr and $K_H=10^{-8}$ m^2 s^{-1}. The amount of water stocked above the interface is directly proportional to this thickness:

$$\int_{-\infty}^{0}([H]-[H]_\infty)\mathrm{d}z=[H]_\infty\frac{1-D}{D}\frac{\kappa_H}{u_z}. \qquad (8)$$

It decreases as the velocity increases. The time necessary to transport the same amount of water across the interface is given by Eq. 8 divided by the velocity, u_z. It lies in the range of a few thousand years for $u_z=1$ cm/yr and $K_H=10^{-8}$ m^2 s^{-1}, suggesting a water transport by advection larger than the diffusion transport by several orders of magnitude. Nevertheless, we might expect strong variations in water concentration at the boundary between two layers with different solubility, whatever the partitioning between both modes of transport.

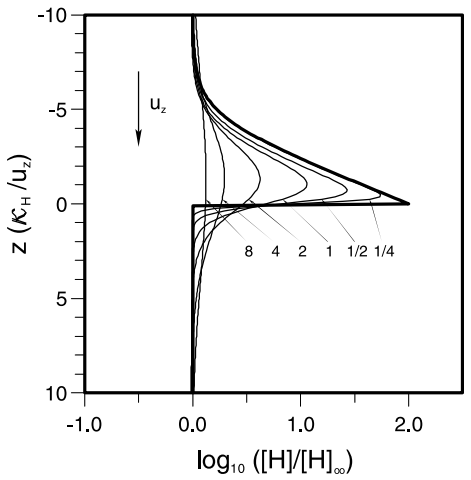

Fig. 2. Influence of the normalized phase change half thickness σ on the shape of the water concentration above a phase change with a water partition coefficient of 100. The normalized water concentration is plotted as a function of K_H/u_z. K_H/u_z represents the characteristic thickness of the water accumulation. We see that the higher the value of σ, the less water is concentrated near the interface. Note also that an increase of K_H and a decrease of u_z will play the same role and make the high concentration zone thicker.

In fact, the strength of this barrier effect depends on the sharpness of the variation in pure material chemical potential, μ^*, and therefore on the thickness of the phase change. In the Earth's mantle, the phase changes probably do not occur in a discontinuous way. In our model the phase change thickness is prescribed through the parameter σ. When μ^* is defined by Eq. 6, Eq. 4 has to be solved numerically. The thin curves on Fig. 2 show the solutions for σ ranging from $0.25\times K_H/u_z$ to $8\times K_H/u_z$. The barrier effect persists as long as the phase transition remains thinner than K_H/u_z, but the amplitude of the water accumulation strongly decreases for thicker phase transition. It reduces by one order of magnitude when $\sigma=K_H/u_z$ and two orders of magnitude when $\sigma=8\times K_H/u_z$.

Seismic estimates of the width of the mantle discontinuities infer a very sharp phase transition at 400 km, less than 5–7 km, and a thicker one at 650 km, 20–30 km [26]. They are globally lower than thermomechanical estimates [27]. The 650 km phase transition is expected to have the larger

influence on the water distribution, because of the two orders of magnitude contrast in the water solubility existing between transition zone and lower mantle minerals. Consequently, its thickness would strongly restrict the effect of the solubility variation.

These effects should be only perceptible along parts of the discontinuity where the mantle vertical mass flux is almost non-existent: the vertical velocity should be less than 3×10^{-2} mm/yr ($K_H/u_z > \sigma$, taking σ, the half thickness of the phase transition, equal to 10 km and $K_H = 10^{-8}$ m^{-2} s^{-1}).

2.4. Time dependence

We will now neglect the advection term in Eq. 4 and focus on the time-dependent solutions. Fig. 3 displays the time evolution of water concentration under the effect of pure diffusion. The domain corresponds to the whole mantle and contains three layers: the upper mantle, the transition zone and the lower mantle associated with the variation in pure material chemical potential displayed in Fig. 1. We used 512 grid points along the depth so as to preserve a transition thickness in the range of 20 km, σ being at least equal to two mesh sizes ($dz = 5.9$ km, $\sigma = 11.8$ km for a transition thickness of 23.6 km).

Starting from a homogeneous water concentration, the equilibrium state is reached when the concentration ratio between layers equals the solubility ratio. This happens after a non-dimensional time in the order of 1. In the absence of mantle convection, the time scale is based on the water diffusivity and can be resized by the factor L^2/K_H, where L is the length scale, i.e. the whole-mantle thickness. The intra-grain water diffusivity of the mantle, estimated to be around 10^{-8} m^2 s^{-1} at 1400°C [2], leads to a time scale of around 30 000 Gyr. A relaxation time comparable with the Earth's age would be obtained with a water diffusivity value four orders of magnitude higher. We may note that the upper mantle and the transition zone balance each other after a non-dimensional time of 10^{-2}, which corresponds to the characteristic time based on their own thickness.

In the light of these preliminary results, we may infer that, even if the diffusivity of water is several orders of magnitude larger than those of other chemical elements, it appears too small to affect strongly the mixing expected from the mantle convection. As a consequence, a study including mantle dynamics is necessary to draw conclusions concerning the ability of the transition zone to trap a large amount of water.

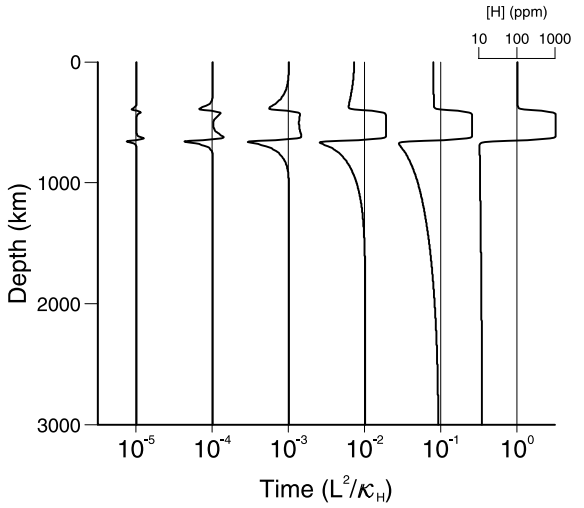

Fig. 3. Pure diffusion effect on mantle water distribution. Here we display the dimensionless temporal evolution of water concentration along the z-axis (depth), according to diffusion process alone. The initial water concentration condition is a homogeneous mantle. During evolution, water content of the upper mantle passes by a minimum that implies a transfer of water from the lower mantle to the upper mantle. Non-dimensional time is L^2/K_H where $L = 3000$ km is the thickness of the mantle and K_H is the water diffusivity. With high diffusivity, $K_H = 10^{-6}$ m^2 s^{-1}, distribution reaches steady state, the equilibrium profile, after 300 billion years; two orders of magnitude greater than Earth's age. This experiment shows the slowness of the diffusion process to enrich water in the transition zone.

3. Influence of mantle dynamics

3.1. Equations of convection

The velocity field, **u**, used to solve the water conservation Eq. 4 derives from a numerical model of mantle convection, which is based on the usual hydrodynamic equations in the approximation of infinite Prandtl number:

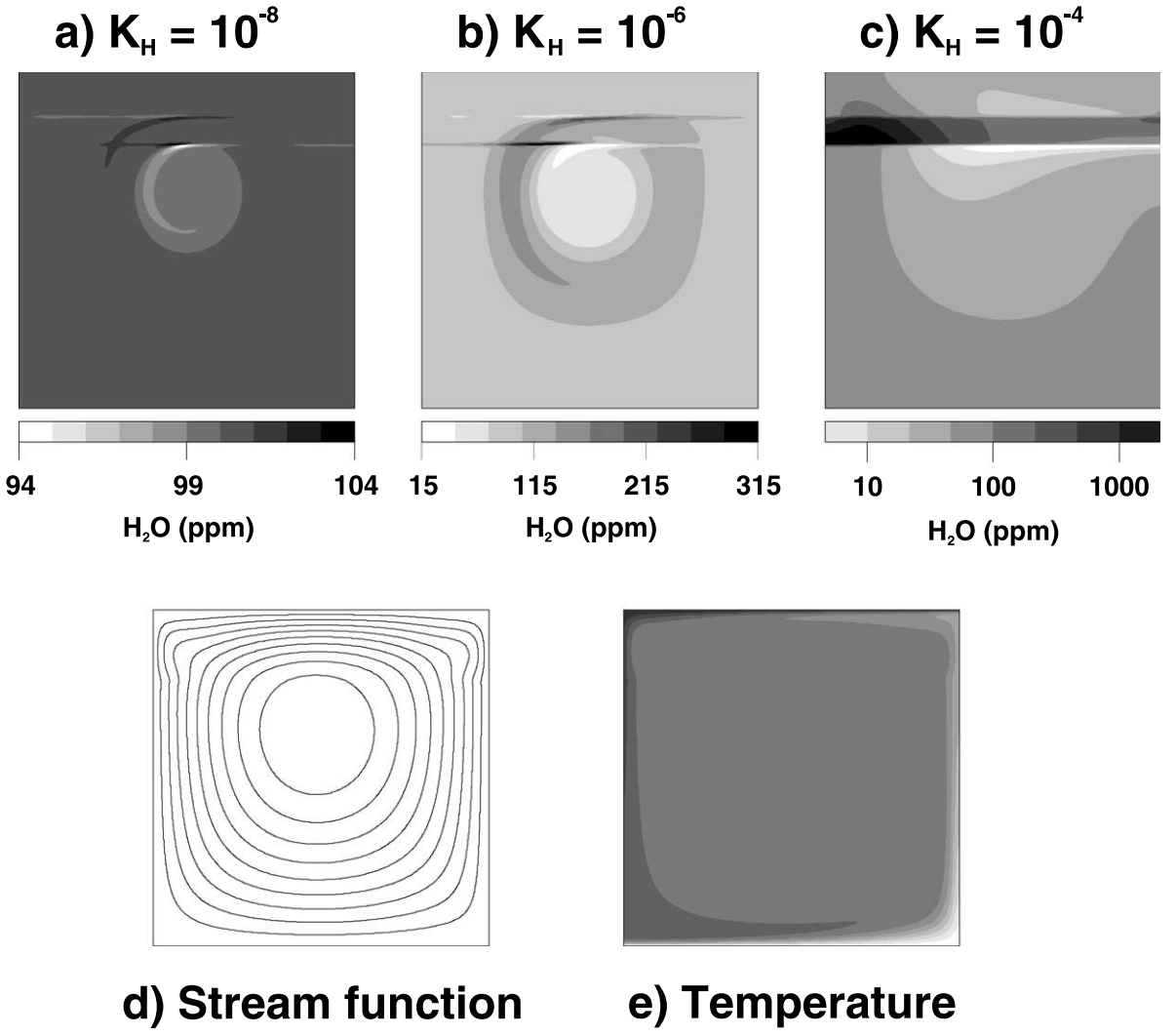

Fig. 4. Influence of water diffusivity on water concentration variations. (a), (b), (c) display the snapshots of the water content in ppm after convergence is supplied for different water diffusivities, (d) is the stream function corresponding to the temperature field (e). A Rayleigh number of 10^6 and a free slip condition at the top of the box are applied to a homogeneous water content mantle. Concentration variation in the high diffusivity case $K_H = 10^{-6}$ m^2 s^{-1} reaches a factor of 10 (b), but remains too low to be discernible for this range in the low diffusivity case $K_H = 10^{-8}$ m^2 s^{-1} (a). In these two cases, maximum variations settle near the center of the convection cell where the vertical velocities are the lowest. With very high water diffusivity $K_H = 10^{-4}$ m^2 s^{-1} (c) the enriched zone is localized in the downward flow area where the contrast reaches a value of 500 exceeding the maximum factor of 100 in the pure diffusion case (Fig. 3).

$$\nabla\cdot\mathbf{u} = 0, \tag{9}$$

$$-\nabla p - \rho\alpha T\mathbf{g} + \eta\Delta\mathbf{u} = \mathbf{0}, \tag{10}$$

$$\frac{\partial T}{\partial t} + \mathbf{u}\cdot\nabla T = \nabla\kappa\cdot(\nabla T) + \Phi. \tag{11}$$

Here p denotes the pressure, ρ the mean density, α the thermal expansivity, $\mathbf{g}$ the gravity, η the viscosity, T the temperature, K the thermal diffusivity and Φ the internal heat generation. The velocity field is expressed in terms of a stream function Ψ through:

$$u_x = \frac{\partial \Psi}{\partial z} \text{ and } u_z = -\frac{\partial \Psi}{\partial x}. \quad (12)$$

Introducing Eq. 12 in the momentum Eq. 10 leads to the fourth-order differential equation of the stream function:

$$\Delta^2 \Psi = -\frac{\rho g \alpha}{\eta} \frac{\partial T}{\partial x}. \quad (13)$$

The boundary conditions for both the energy and momentum equations will be explained in the next section, as they vary from one experiment to another. Every experiment has been performed with a stepwise increase in viscosity by a factor of 30 across the 650 km discontinuity. Such a viscosity variation has been put forward to account for the geoid–topography relationship at long wavelengths [28].

Using finite differences and the alternate direction implicit (ADI) scheme, the water and energy equations are solved over a regular grid using the method developed by Douglas [29]. The mesh size is 11.75 km × 5.875 km (512 grid points along the vertical direction). The stream function is expanded in Fourier series and solved by finite differences along the vertical direction over 512 points.

3.2. *Influence of water diffusivity and water solubility*

Now, we can proceed to a 2-D cartesian model, firstly by looking at the effects on the water distribution of the steady-state velocity field of a simple square convection cell (Fig. 4d and e). Top and bottom boundaries are free slip, and there is no internal heating. The Rayleigh number is set to 1.1×10^6 so that the surface velocity reaches 3.5 cm/yr in average, which is comparable to the Earth's plate velocities. Note, on the stream function and the temperature field, the narrowing of the isolines due to the presence of the viscosity gradient at 650 km. Fig. 4a, b and c displays the steady-state water distribution obtained for three different values of water diffusivity: 10^{-8}, 10^{-6} and 10^{-4} m^2 s^{-1} respectively, from a homogeneous content of around 100 ppm. In the three cases, the time required to reach the steady state is smaller ($K_H = 10^{-8}$, 10^{-6} m^2 s^{-1}) or of the same order ($K_H = 10^{-4}$ m^2 s^{-1}) than the time scale based on the water diffusivity (roughly 15 Gyr). For the smallest value of the water diffusion, 10^{-8} m^2 s^{-1} (Fig. 4a), the variation in water content remains negligible below 10 ppm and the solubility jumps are likely to have no effect. For the intermediate value, 10^{-6} m^2 s^{-1} (Fig. 4b), the distribution pattern looks similar to the former but with larger amplitude. The most water-enriched and depleted zones are focused on either side of the boundaries of the transition zone and horizontally restricted to the region where the vertical velocity is low enough to allow the diffusion process to act, i.e. at the horizontal middle part of the cell. The maximum contrast between high and low water content reaches a factor of 15 in low water content area (TZ–LM boundary). It is necessary to increase the water diffusivity up to 10^{-4} m^2 s^{-1} (Fig. 4c) to observe strong variations in the water distribution. In this case, the pattern is quite different from the previous ones. The enriched zone is localized in the high solubility zone (the transition zone) of the downward flow region. Surprisingly, the range in the water content reaches around 5000 ppm. This exceeds the maximum contrast of 990 ppm expected in case of pure diffusion. In Fig. 5, this range has been plotted as a function of water diffusivity. It exhibits a maximum for a value of water diffusivity of 10^{-4} m^2 s^{-1}, suggesting a resonance phenomenon between the convection and diffusion time scale.

The preliminary conclusion of this first series of experiments is that a high water solubility zone seems efficient in storing a significant amount of water only for high water diffusivity; a diffusivity four orders of magnitude higher than the one determined from laboratory experiments. Nevertheless, mantle dynamics are much more complex than the case used in this oversimplified experiment, and a more realistic model must be used to draw robust conclusions.

3.3. *The role of mantle dynamics in water distribution through the Earth's mantle*

The Earth's mantle dynamics are mostly controlled by plate tectonics [30]. To simulate this system, a model of mantle convection would re-

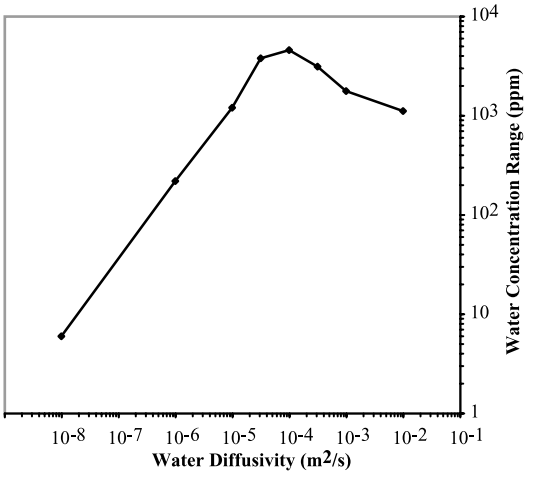

Fig. 5. Maximum water concentration range reached at steady state as a function of water diffusivity (i.e. difference between maximum and minimum H_2O concentration) in model presented in Fig. 4. The contrast is maximum for a diffusivity value of $K_H = 10^{-4}$ m^2 s^{-1}. This value exceeds the one expected without convection and may correspond to a resonance between the effects of convection and diffusion.

quire a top boundary condition, which more closely represents plate dynamics than the free slip condition previously used. Such a boundary condition was proposed by Ricard and Vigny [28] and will be adopted in the following experiment. The method consists of a piece-wise rigid condition: each part of the top boundary mimics a plate and is free to move in the positive or negative direction. The velocity of each plate is assumed to be constant over the first 80 km and is calculated at each iteration by balancing stresses exerted by the mantle convection with stresses induced by the plate motion. In this model, plate geometry remains fixed during the whole experiment. Additionally, the model will be performed with pure internal heating. In doing so, we focus the experiment on the dynamics of plates and subductions, neglecting the effect of a hot mantle plume. All other parameters have been chosen so that the surface velocities should be in the range of Earth's plate velocities, i.e. 4 cm/yr on average.

In the experiment displayed in Fig. 6, three tectonic plates constitute the top boundary. One extends over 7000 km, which is representative of the average plate length on Earth. The aspect ratio of the box is 5 (1280×512 grid points). In Fig. 6, a panel series displays the temperature field evolution over four billion years. The surface velocity is plotted above each panel. The subduction zone appears to jump from one plate boundary to an other with time. This switching is only derived from the 2-D framework of the model, and is not observed in 3-D spherical geometry, where the sinking currents slowly move around the plates [30]. However, this artifact is useful to reproduce the unsteady behavior of mantle convection.

Using this model of mantle convection, we will now compare two evolutions starting with opposite distributions (Fig. 7): a homogeneous water content and the relaxed one obtained at the diffusion equilibrium, i.e. the distribution fits the partition coefficient 1:10 for UM/TZ and 1:100 for LM/TZ shown in Fig. 1. We assume there is no external water source, so the total amount of water will remain constant in the box and will be fixed to the same value in both cases. To start with the same total amount in both cases, the initial condition is a water content of 100.3 ppm everywhere in the first case and an equilibrated distribution of 10 ppm in the lower mantle, 1000 ppm in the transition zone and 100 ppm in the upper mantle, in the second case. Lastly, to take into account possible grain boundary diffusion, the water diffusivity is set at a high value of 10^{-6} m^2 s^{-1} [27]. It will emphasize the effect of the diffusion process and of the solubility variation that was very weak with K_H of 10^{-8} m^2 s^{-1}.

The early evolution of the water content, depicted in Fig. 7, highlights the strong mixing induced by the convection and the inability of the diffusion process to concentrate or to keep the water in the high solubility region, i.e. the transition zone.

In the case where the initial condition is a homogeneous distribution (Fig. 7, left-hand side), only a weak variation appears after 100 Myr. In the region of the transition zone crossed by the subduction, the diffusion effect is erased. Elsewhere, the transition zone pumps water. Near the upper interface (UM/TZ) the concentration is a maximum but remains less than 200 ppm. In the other case (Fig. 7, right-hand side), the

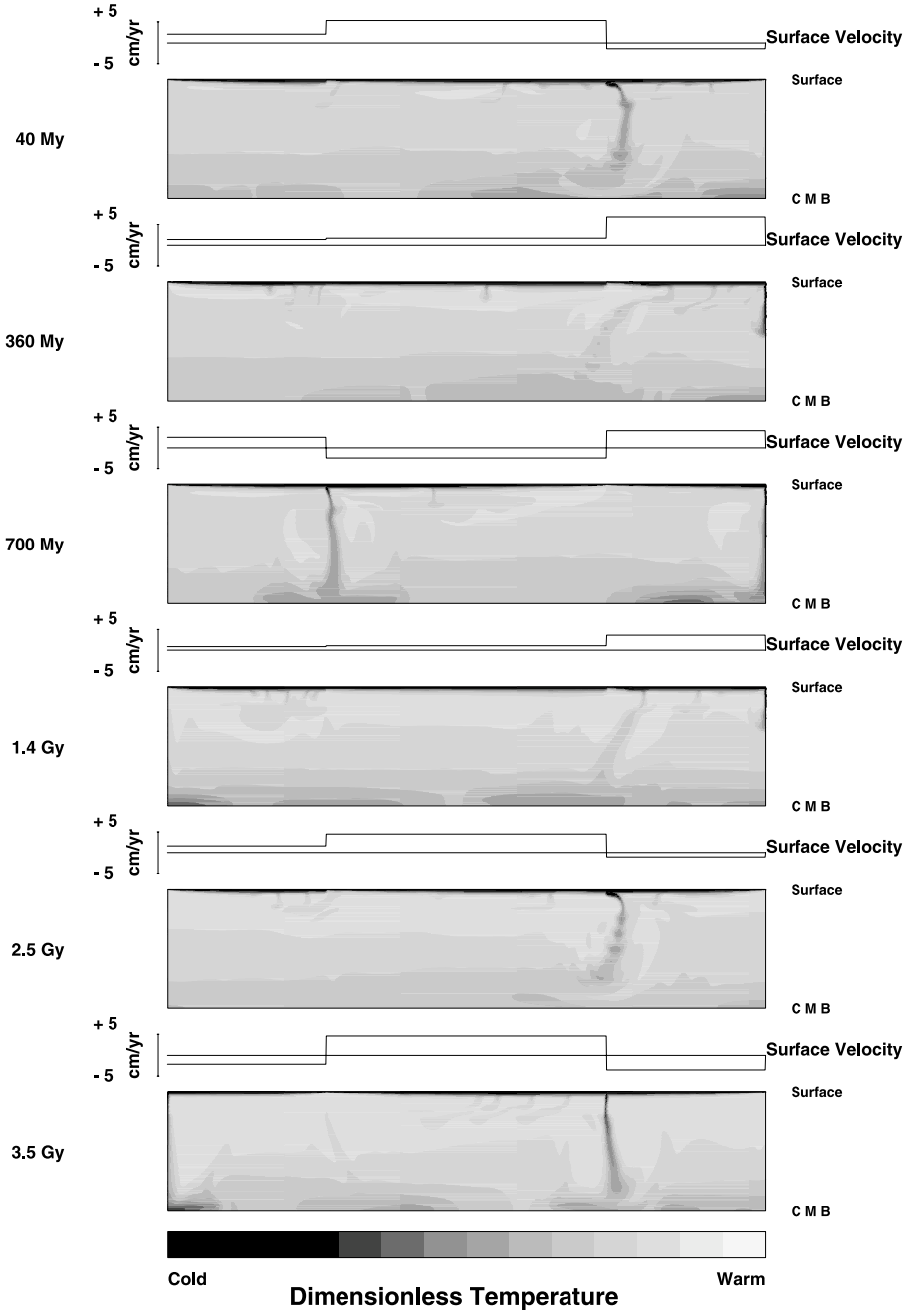

Fig. 6. Snapshots of dimensionless temperature fields in a convecting mantle. Figures show the temporal evolution of the temperature in a 2-D cartesian box of 3000 km depth. Surface conditions are imposed as zero temperature and three tectonic plates velocity. Plate motion is controlled by stresses induced by the convection [29]. Bottom conditions are zero heat flux and free slip. The velocity field corresponding to this temperature field is used in H_2O transport calculations presented in Figs. 7 and 8.

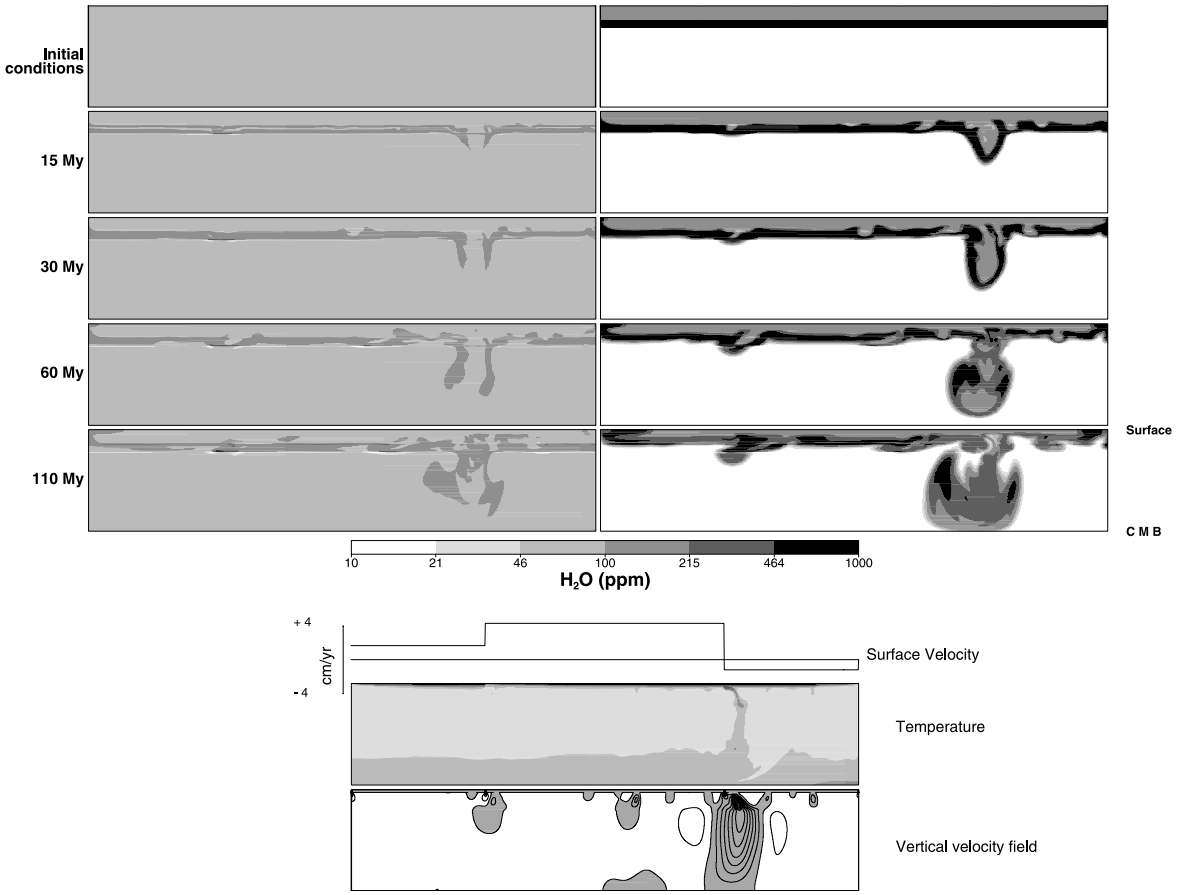

Fig. 7. Evolution of water distribution in Earth's mantle starting from two different initial conditions: a homogeneous initial mantle (left-hand side) and an initial mantle at diffusive equilibrium (right-hand side). Water contained in transition zone (TZ) is driven downward to the lower mantle by the advecting flow. Due to the very low solubility in lower mantle, water saturation can be expected and free water would be released just under the transition zone. The dimensionless temperature and vertical velocity fields corresponding to 30 Myr are also displayed to help the Localization of the subduction zone. In the latter, the negative velocities area is shaded in dark and the positive in light. The step between isolines is 1 cm/yr.

horizontal stratification set at the beginning is completely removed by the subducting flow. The water present in the transition zone at the initial state is advected and dispersed in the lower mantle by the downward flow. Away from the subduction zone, the stratification is preserved during the first 30 Myr. After 100 Myr, this horizon has been stirred and dragged toward the upper mantle by the diffuse upward flow, especially at the ridges, and only some residual pockets of high water content remain in the vicinity of the transition zone.

Fig. 8 displays the evolution over billion-year intervals. If in the homogeneous case (Fig. 8, left-hand side) the distribution evolves with time, the main features remain the same during four billion years. Some enriched regions remain close to the interfaces and the maximum contrast never exceeds a factor of 3, far from the factor of 100 imposed by the partition coefficients. In the second case (Fig. 8, right-hand side) some large lateral heterogeneity can still be observed but the horizontal layered distribution is no longer discernible. Finally, after four billions years, the water distribution appears quite homogeneous and the differences between higher and lower con-

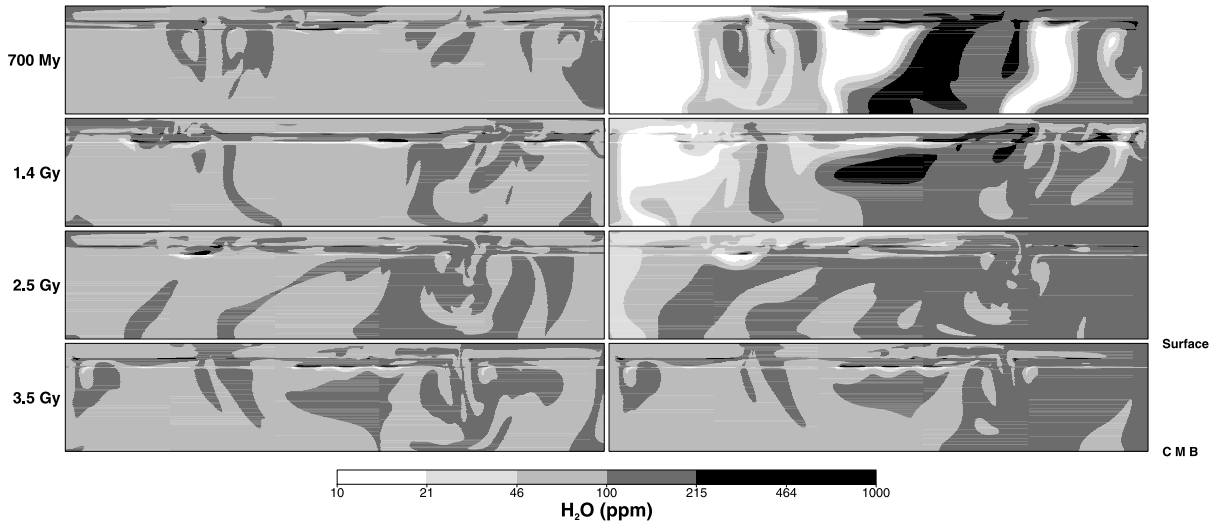

Fig. 8. Long-term evolution of water distribution in Earth's mantle starting from two different initial conditions (next to Fig. 7). After three billion years, the water content variations in both cases are similar. The initial conditions are no longer discernible.

centrations are comparable with the result obtained using the homogeneous initial condition. The comparison between these two experiments demonstrates that in a case with a relatively high water diffusivity, initial conditions of water distribution have no effect on the water distribution in the long term and that the mixing effect provided by mantle convection is a dominant process.

3.4. Effects of a source term

In previous experiment, because of the absence of a source term in the water equation, subduction zones are dry. Actually, subducting plates drag hydrated crust into the mantle. Most of this water is released in the mantle wedge when hydrous minerals leave their stability field, but the remaining part is driven deeper and constitutes a water source for the mantle. We handle with the positive source term by imposing a constant concentration equal to a dimensionless unit at the convergence of two plates. In this experiment, the initial state is zero water content everywhere in the mantle. Fig. 9 shows from top to bottom: water concentration evolution during 60 Myr, a snapshot of the temperature field taken after 30 Myr of evolution and a snapshot of the corresponding vertical velocity field. This field is representative of Earth subduction, around 5 cm/yr.

It is notable that solubility variation has little effect on the water advected by subducting plates for a diffusivity of 10^{-6} m^2 s^{-1}. All the water is directly led to the core–mantle boundary and crosses the transition zone, as there is no solubility change. These experiments let us assume that, in the absence of transport processes other than diffusion and advection, subducted water will be driven to the core–mantle boundary and follow the path of the recycled oceanic crust.

4. Concluding remarks

The essential outcome of the experiments described here is that advection is likely to control water distribution, even with the assumption that grain boundary diffusion enhances the diffusion rate by two orders of magnitude (10^{-6} m^2 s^{-1}) [27]. The assumption we have made to neglect the temperature dependence of the water diffusivity is justified by this result, since its effect will be to decrease the diffusivity in some regions. Here, we did not take into account the 660 km phase changes in the convection model and so we did not approach the case of layered convection. In

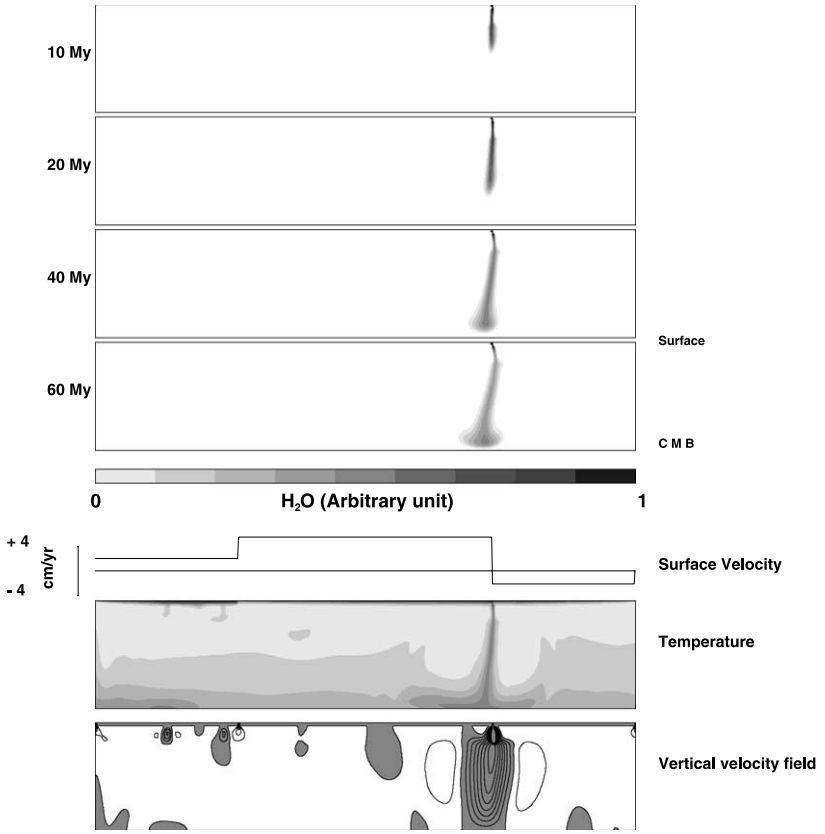

Fig. 9. Behavior of subducting water. The temporal evolution of water distribution in Earth's mantle with a water source at the trench. The two lower figures show temperature and vertical velocity fields corresponding to 30 million years and are representative of the entire evolution presented above. Water injected at the trench into an empty mantle is directly driven through the mantle to the core–mantle boundary (CMB). As the water crosses the TZ, the diffusion process (with $K_H = 10^{-6}$ m^2 s^{-1}) is not efficient enough to pump water from the subducting flow to the TZ.

this case, a subducted slab or part of it can stay long enough in the transition zone [31]. When we force the convection to be stratified then the transition zone is water-enriched in a first stage and then water content of the transition zone and the upper mantle is homogenized. The effect of the 1:10 partition coefficient between UM and TZ is quite invisible like in the whole-mantle convection cases. In this one convection layer case, the transition zone is likely to have no influence on water dynamics. Indeed, water coming from the transition zone or from a subduction zone can be lead into the lower mantle (Fig. 9, right-hand side Fig. 7).

However, if no extra hydrous or hydrous rich minerals are stable in the lower mantle, as it is suggested by high-pressure experiments [3], water solubility in lower mantle is very low. Therefore some parts of the lower mantle could be water supersaturated and so free water could be produced in these areas. We must ask what is the behavior of water driven by dynamic flows deeper than the transition zone? One possibility is that free water remains confined as fluid inclusions or as hydrous phases in rocks. In that case, water may be lead to the core–mantle boundary (Fig. 9) and stay there during several hundred million years. The presence of a significant amount of water at the core–mantle boundary could explain some seismic characteristics of the D'' layer. It could also explain the high water content of hot spot basalts since hotspots could appear at the

core–mantle boundary. Here we must recall that our model assumes a zero water flux between core and mantle. A more probable possibility is the release of water by rocks during the transformation of spinel into perovskite plus magnesiowustite and then free water should be present at grain boundaries. This question can be related to the behavior of water contained in the hydrous minerals of a subducting slab. At lower depths, we know that water expelled from hydrous mineral is likely to migrate and to trigger melting which is the source of arc magmatism [32]. Actually, the behavior of water is probably the same in both cases and we can guess that free water is produced below subduction zones at the top of the lower mantle.

Further work is needed to establish the distribution induced by free water percolation, but we can guess that water in a porous medium will behave like magma described by Stevenson, in 1989 [33]. Water or magma would migrate along the direction parallel to the axis of minimum compressive stress and accumulate in veins. Then buoyancy would drive the water back up to the transition zone. The distribution provided in a very high diffusivity experiment (right-hand side Fig. 4) is likely to give a good estimate of the distribution induced by water percolation. Concentration should be very high above the TZ/LM interface, water partitioning could be higher than the 1:100 expected from the solubility jump. It could be a very efficient way to concentrate water and to produce a water-rich zone in the Earth's mantle. But to decide between these two hypotheses, further high-pressure experiments must be performed to confirm if water cannot be effectively stored in the lower mantle NAMs. Finally, this study highlights the probable importance of free water behavior on water distribution in the Earth's mantle.

Acknowledgements

We thank Michel Rabinowicz and Marc Blanchard for early discussions and encouragements. We also thank Yanick Ricard for helpful comments on the first version of this paper. Finally, we are grateful to Ester Harris for her English review. *[BW]*

Appendix

We have used the high-resolution 1-D model to check the stability of the numerical solution computed on a coarser grid. Fig. 2 shows that the numerical solution with 16 384 grid points tends to the analytical one (thick curve) when σ tends to zero. Furthermore, the accuracy of the solution can be checked with an internal criterion. At steady state Eq. 4 gives:

$$\frac{\partial}{\partial z}\left(\kappa_{\mathrm{H}}\frac{\partial}{\partial z}[H]+\kappa_{\mathrm{H}}\left([H]\frac{\partial}{\partial z}\frac{\mu_i}{RT}\right)-u_z[H]\right)=0 \quad \text{(A1)}$$

that expresses the conservation of the water flux along z. When z tends toward $-\infty$, this flux is equal to $-u_z[H]_\infty$, so that:

$$\kappa_{\mathrm{H}}\left(\frac{\partial}{\partial z}\ln[H]+\frac{\partial}{\partial z}\frac{\mu_i}{RT}\right)=u_z\frac{[H]-[H]_\infty}{[H]}. \quad \text{(A2)}$$

After integration over the whole domain, we find that:

$$\frac{u_z}{\kappa_{\mathrm{H}}}\int_{-\infty}^{+\infty}\frac{[H]-[H]_\infty}{[H]}\mathrm{d}z=\frac{\Delta\mu}{RT} \quad \text{(A3)}$$

where $\Delta\mu$ is the difference in pure material chemical potential from $-\infty$ to $+\infty$. The notable interest of this quantity is that it does not depend on the σ, u_z or K_{H}. We find an agreement remaining within 2%, which does not depend on the mesh size as long as $\sigma \geq 2\times \mathrm{d}z$.

References

[1] D.R. Bell, G.R. Rossman, Water in Earth's mantle: The role of nominally anhydrous minerals, Science 255 (1992) 1391–1397.
[2] J. Ingrin, H. Skogby, Hydrogen in nominally anhydrous upper mantle minerals: Concentration levels and implications, Eur. J. Mineral. 12 (2000) 543–570.
[3] N. Bolfan-Casanova, H. Keppler, D.C. Rubie, Water partitioning between nominally anhydrous minerals in the MgO-SiO_2-H_2O system up to 24 GPa: implications for the distribution of water in Earth's mantle, Earth Planet. Sci. Lett. 182 (2000) 209–221.
[4] D.L. Kohlstedt, H. Keppler, D.C. Rubie, Solubility of

water in the alpha, beta and gamma phases of (Mg,Fe)(2)SiO_4, Contrib. Mineral. Petrol. 123 (1996) 345–357.
[5] A.B. Thompson, Water in the Earth's upper mantle, Nature 358 (1992) 295–302.
[6] Q. Williams, R.J. Hemley, Hydrogen in the deep Earth, Annu. Rev. Earth Planet. Sci. 29 (2001) 365–418.
[7] T. Inoue, Effect of water on melting phase relations and melt composition in the system Mg_2SiO_4-$MgSiO_3$-H_2O up to 15 GPa, Phys. Earth Planet. Int. 85 (1994) 237–264.
[8] G. Hirth, D.L. Kohlstedt, Water in oceanic upper mantle – implications for rheology, melt extraction and the evolution of lithosphere, Earth Planet. Sci. Lett. 144 (1996) 93–108.
[9] I. Kushiro, Effect of water on composition of magmas formed at high pressures, J. Petrol. 13 (1972) 71–136.
[10] C.W. Burnham, in: H.L. Barnes (Ed.), Geochemistry of Hydrothermal Ore Deposit, 2nd edn., Wiley, New York, 1979, pp. 71–136.
[11] S. Karato, Effect of water on the seismic wave attenuations the upper mantle, Proc. Jpn. Acad. Ser. B 71 (1995) 61–66.
[12] B.J. Wood, The effect of H_2O on the 410-kilometer seismic discontinuity, Science 268 (1995) 74–76.
[13] P.N. Chopra, M.S. Paterson, The role of water in the deformation of dunite, J. Geophys. Res. 89 (1984) 7861–7876.
[14] S. Karato, The role of hydrogen in the electrical conductivity of the upper mantle, Nature 347 (1990) 272–273.
[15] S. Karato, Mapping Water Content in the Upper Mantle, The Subduction Factory, AGU Monograph, in press.
[16] C. Lecuyer, P. Allemand, Modelling of the oxygen evolution of the see water: implications for the climate interpretation of the $\delta^{18}O$ of marine sediments, Geochim. Cosmochim. Acta 63 (1999) 351–362.
[17] G. Schubert, A.P.S. Reymer, Continental volume and freeboard through geological time, Nature 316 (1985) 336–339.
[18] E. Bonatti, Not so hot 'Hotspots' in the oceanic mantle, Science 250 (1990) 107–111.
[19] J.E. Dixon, E.M. Stolper, J.R. Holloway, An experimental study of water and carbon dioxide solubilities in mid ocean ridge basaltic liquids. Calibration and solubility models, J. Petrol. 36 (1995) 1607–1631.
[20] J.R. Smyth, D.R. Bell, G.R. Rossman, Incorporation of hydroxyl in upper-mantle clinopyroxenes, Nature 351 (1991) 732–735.
[21] L. Stixrude, Mineral physics of the mantle, Rev. Geophys. Suppl. 33,
[22] T. Inoue, H. Yurimoto, Y. Kudoh, Hydrous modified spinel $Mg_{1.5}SiH_{0.5}O_4$: a new water reservoir in the mantle transition region, Geophys. Res. Lett. 22 (1995) 117–120.
[23] E. Ohtani, M. Toma, K. Litasov, T. Kubo, A. Suzuki, Stability of dense hydrous magnesium silicate phases and water storage capacity in the transition zone and lower mantle, Phys. Earth Planet. Int. 124 (2001) 105–117.
[24] S.R. De Groot, P. Mazur, Non-equilibrium Thermodynamics, Dover Publication, New York, 1984, pp. 275–247.
[25] L. Landau, E. Lifchitz, Physique Statistique, Editions Mir, Moscow, 1967, pp. 335–342.
[26] N. Petersen, L. Vinnik, G. Kosarev, R. Kind, S. Oreshin, K. Stammler, Sharpness of the mantle discontinuities, Geophys. Res. Lett. 20 (1993) 859–862.
[27] J.R. Smyth, D.J. Frost, The effect of water on the 410-km discontinuity: An experimental study, Geophys. Res. Lett. 29 (2002) 10.1029/2001GL014418.
[28] Y. Ricard, C. Vigny, Mantle dynamics with induced plate tectonics, J. Geophys. Res. 94 (1989) 17543–17559.
[29] J. Douglas, G. Rachford, On the numerical solution of heat conduction problems in two and three space variables, Trans. Am. Math. Soc. 82 (1956) 421–439.
[30] M. Monnereau, S. Quere, Spherical shell models of mantle convection with tectonic plates, Earth Planet. Sci. Lett. 184 (2001) 575–587.
[31] S. Karato, M.R. Riedel, D.A. Yuen, Rheological structure and deformation of subducted slabs in the mantle transition zone: implications for mantle circulation and deep earthquakes, Earth Planet. Sci. Lett. 127 (2001) 83–108.
[32] P. Ulmer, V. Trommsdorff, Serpentine stability to mantle depths and subduction-related magmatism, Science 268 (1995) 858–861.
[33] D.J. Stevenson, Spontaneous small-scale melt segregation in partial melts undergoing deformation, Geophys. Res. Lett. 16 (1989) 1067–1070.